Journal of Electron Microscopy **58(3)**: 167–174 (2009)
doi: 10.1093/jmicro/dfp003

Special number: Methods

Three-dimensional shapes and structures of lamellar-twinned fcc nanoparticles using ADF STEM

Lionel C. Gontard[1,2,*], Rafal E. Dunin-Borkowski[1,2], Mhairi H. Gass[3], Andrew L. Bleloch[3] and Dogan Ozkaya[4]

[1]Center for Electron Nanoscopy, Technical University of Denmark, DK-2800 Kgs. Lyngby, Denmark, [2]Department of Materials Science and Metallurgy, University of Cambridge, Pembroke Street, Cambridge CB2 3QZ, UK, [3]SuperSTEM Laboratory, Daresbury Laboratory, Daresbury WA4 4AD, UK and [4]Johnson Matthey Technology Centre, Blount's Court, Sonning Common, Reading RG4 9NH, UK
*To whom correspondence should be addressed. E-mail: lionel.gontard@cen.dtu.dk

Abstract Small particles with face-centred cubic structures can have non-single-crystallographic shapes. Here, an approach based on annular dark-field scanning transmission electron microscopy (STEM) is used to obtain information about the crystal sub-units that make up supported and unsupported twinned Pt, Pt alloy and Au nanoparticles. The three-dimensional shapes of two types of lamellar-twinned particles (LTPs) of Pt are obtained using high-angle annular dark-field STEM. Possible growth mechanisms of the LTPs and origins for the contrast features in the recorded images are discussed.

Keywords heterogeneous catalysis, nanoparticles, platinum, platinum alloys, electron tomography, nanoparticle shapes

Received 22 October 2008, accepted 14 January 2009, online 11 February 2009

Introduction

Metal nanoparticles are often used as heterogeneous catalysts and in applications that include plasmonics and nonlinear optics [1,2]. An understanding of their structures is important, both because their chemical, electronic and optical properties can be very different from those of bulk single crystals, and for understanding their growth dynamics. For example, single nanocrystals of silver are found to have better catalytic activity and reduced electron–phonon coupling when compared with twinned nanocrystals [3].

The structures, shapes and growth mechanisms of metallic nanoparticles have been studied intensively both theoretically and experimentally [4,5]. Although the thermodynamically stable shape of a nanoparticle should correspond to a Wulff construction, a nanoparticle with a small number of atoms need not have a fixed structure at a given temperature, but may be fluctuating dynamically between different shapes [6]. The appearance of a single structure at equilibrium may be indicative of a minimum in the total free energy of the particle, with both surface and bulk energy terms included. A phase diagram derived for small gold particles illustrates the fact that different crystal structures can be stable for different particle sizes and temperatures [6]. For gold particles of a given size, a change in the crystal structure, from face-centered cubic (fcc) to decahedral and icosahedral, occurs with increasing temperature. Decahedral and icosahedral crystallites are normally considered to be made up of tetrahedral fcc segments that are joined together in a twinned arrangement. They are then referred to as 'multiply twinned' particles (MTPs). An MTP structure minimizes bulk, surface and interface energies, whereas an fcc structure minimizes just the energy of the bulk structure.

The effects of temperature and particle size, and the presence of adsorbates, have all been found to affect the equilibrium structures of small particles. For Ni, icosahedral structures are favoured slightly when the sizes of nanoparticles are reduced [7]. For Ag and Pt, for which the formation temperature is lower, decahedral and icosahedral structures form [8,9]. Molecular dynamics (MD) simulations are used widely as a tool for studying structural size effects, thermal vibrations and melting [10,11]. Model atomic arrangements can be 'optimized energetically' by allowing atoms to relax in an appropriate self-consistent force field [12]. MD simulations have been used to predict icosahedral structures for Cu nanoparticles with sizes of below 3.8 nm, while an fcc structure is predicted above this size. A 3.8 nm Cu cluster contains ~2500 atoms, of which ~30% are at its surface. In practice, small Au nanoparticles can form many different

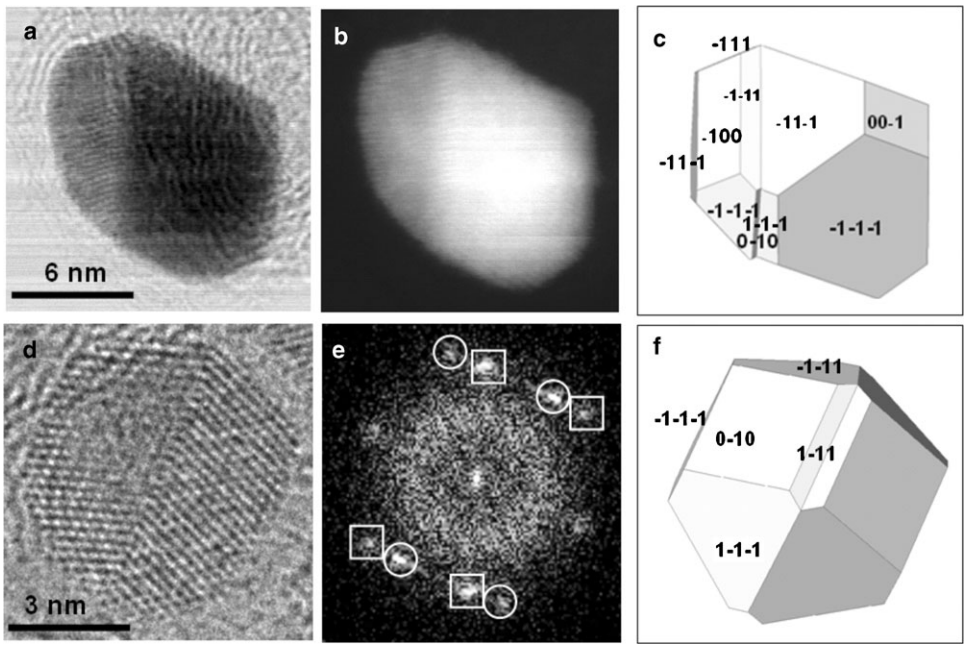

Fig. 1. (a) BF and (b) ADF (~40 mrad inner detector semi-angle) STEM images of an asymmetrically twinned Pt particle acquired at 100 kV. (d) HRTEM image and (e) diffractogram of a symmetrically twinned Pt_3Co particle acquired at 300 kV. (c and f) Inferred possible crystallographic models of the particles shown in (a) and (d), respectively, exhibiting 111- and 100-type facets.

types of twinned particles. These include (i) fcc structures with various morphologies [cuboctahedra (CO), octahedra (Oh), truncated octahedra (TO, TO6) and their twinned variants]; (ii) icosahedra (Ih) and capped-Ih (c-Ih) structures; (iii) hexagonal-close-packed (hcp) structures and (iv) pentagonal decahedral (Dh) arrangements and their variants, including Ino-Dh (i-Dh) and Marks-Dh (m-Dh), in which re-entrant (111) facets are described using a modified Wulff construction [13].

The characterization of twinned nanoparticles was first carried out by studying double-diffraction spots using selected area electron diffraction in a 1000 kV electron microscope [14]. STEM microdiffraction patterns were subsequently used to provide evidence for the presence of twinning in 5 nm Au crystals [15]. Many experimental studies have been carried out by applying high-energy electron diffraction (HEED) to freely floating nanometre-sized nanoparticles, with the aim of identifying the presence of different crystal structures [9,16,17]. However, it is difficult to separate signals from decahedra and icosahedra, and freely floating particle structures may differ from those of supported particles due to metal–support interactions [18]. The primary advantage of using transmission electron microscopy (TEM) over diffraction methods is that it is the only technique that can be used to determine the crystalline structures of individual small particles unambiguously. For example, a particle that contains different crystals may exhibit different diffraction contrast from each sub-unit. Weak-beam dark-field imaging has been used to identify icosahedral structures in Rh particles [19]. MTPs have also been imaged in detail using high-resolution TEM (HRTEM) [20–22]. The primary disadvantage of HRTEM is that it may provide poor statistics resulting from small numbers of observations. Moreover, lattice fringes need not be related simply to crystal structures, and crystal-tilt-dependent image features can be interpreted erroneously as 'relaxations' or 'twinned' regions.

Most studies of twinned particles have involved the examination of MTPs (i.e. decahedral and icosahedral particles). Here, we study both MTPs and nanoparticles that can have a number of parallel twin boundaries and are referred to as 'lamellar-twinned' particles (LTPs). Annular dark-field (ADF) and high-angle (HAADF) scanning transmission electron microscopy (STEM) imaging and tomography are used to characterize both the structures and the three-dimensional shapes of LTPs. Figure 1 shows examples of images of an asymmetrical and a symmetrical LTP. We discuss the shapes, possible growth mechanisms and contrast features of such particles.

Methods

Carbon-supported (Vulcan XC-72R) platinum (19.1 wt%) was prepared using established techniques by impregnating carbon black supports with aqueous hexachloroplatinic acid, as described elsewhere [23]. The samples were further reduced in a N_2-rich atmosphere at 900°C. In part to reduce the overall cost of the catalyst, alloys of Pt with other metals are used frequently. Here, we study 40 wt% Pt_3Co on carbon black, with a Pt:Co atomic ratio of 75:25. The structures of

such particles can change as a function of alloy content and annealing temperature. Three common structures are those of ordered Pt_3Co and PtCo and disordered PtCo [24]. The specimens were prepared as dry powders and spread on holey carbon copper grids. Au nanoparticles from colloid solutions, which had been air dried on holey carbon grids, were also studied.

Experimental data were acquired using a Tecnai F20 Super-Twin field-emission gun (FEG) TEM operated in a STEM mode at 200 kV, using camera lengths corresponding to inner detector semi-angles of ~40 mrad and ~10 mrad. 1024 × 1024 pixel images were acquired using a single-tilt tomography holder from Fischione Instruments, with a maximum tilt range (limited by the microscope goniometer) of ± 80°. The three-dimensional shapes of the particles were obtained using HAADF STEM tomography [25]. The technique has been applied previously for the determination of the shapes of individual Pt nanoparticles [26]. Here, in order to use HAADF STEM tomography to measure the shapes of Pt catalyst nanoparticles with sufficient spatial resolution, magnifications of between 910 kx and 1.8 Mx were used. Alignment and reconstruction of the datasets was performed using the simultaneous iterative reconstruction technique (SIRT) algorithm in Inspect3D software (15–20 iterations proved to be enough to reach convergence). Visualization of the final three-dimensional datasets was performed by using isosurface rendering in Amira V2.3 software.

Atomic-resolution images in TEM and STEM modes were acquired using a C_s-corrected FEI Titan FEG TEM operated at 300 kV and a C_s-corrected VG HB501 dedicated STEM operated at 100 kV. For the VG STEM, the probe convergence semi-angle was 24 mrad. The inner detector semi-angle was 40 mrad for acquiring ADF images and >70 mrad for acquiring HAADF images.

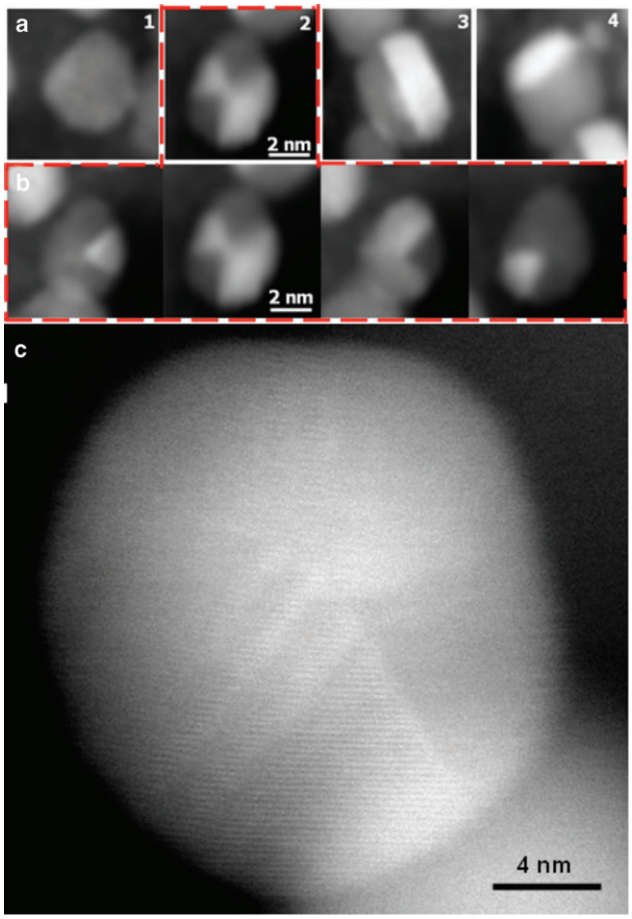

Fig. 2. (a) ADF images (~10 mrad inner detector semi-angle at 200 kV) of (1) a single crystal; (2) a 5-fold MTP; (3) a symmetrically twinned crystal and (4) an asymmetrically twinned crystal. (b) Four ADF images of the MTP particle numbered (2) in (a) acquired at different tilt angles. Different crystal domains appear bright or dark depending on the diffracting condition. (c) High-resolution ADF image of a decahedral Au nanoparticle acquired using an inner detector semi-angle of ~40 mrad at 300 kV.

Results and discussion

Structural characterization of twinned particles using ADF STEM

High-tilt series of low-angle ADF STEM images were used to characterize nanoparticle structures. A low collection semi-angle (~10 mrad) was used to enhance diffraction contrast. Images were typically acquired over tilt ranges of ± 50°, with a 1–4° tilt increment. By using this approach, individual crystal domains in the nanoparticles could be detected and imaged rapidly with a high signal-to-noise ratio and a large field of view. Figures 2 and 3 show selected images taken from tilt series of ADF STEM images of Pt and Pt_3Co nanoparticles supported on carbon. The background contrast from the carbon support is minimized in these images, when compared to using BF STEM imaging.

The images in the top row of Fig. 2 illustrate the most common types of crystalline structures found in the present experiments, corresponding to decahedral structures, single crystals with truncated octahedral morphologies and their symmetrically twin-faulted variants. Interestingly, images such as those in Fig. 2 show the three structure types that are also determined theoretically for 1.4–3.0 nm Au nanoparticles via exhaustive searches and energy-minimization methods compared with data from synchrotron X-ray diffraction [27]. The middle row of Fig. 2 shows four ADF images of the same 5-fold MTP acquired at different tilt angles, confirming the crystallite's ~5-fold symmetry and the presence of five distinct tetrahedral sub-units. Figure 3 shows a series of ADF STEM images taken from two tilt series of Pt_3Co and Pt samples supported on carbon. The top two rows show a 10 nm Pt_3Co particle that contains two crystal domains of different size, referred to as an asymmetrically twinned particle. The bottom row of images shows variations in contrast in a Pt particle, which may be either an MTP or an LTP. Although the collection angle of the ADF detector used to acquire the top two rows

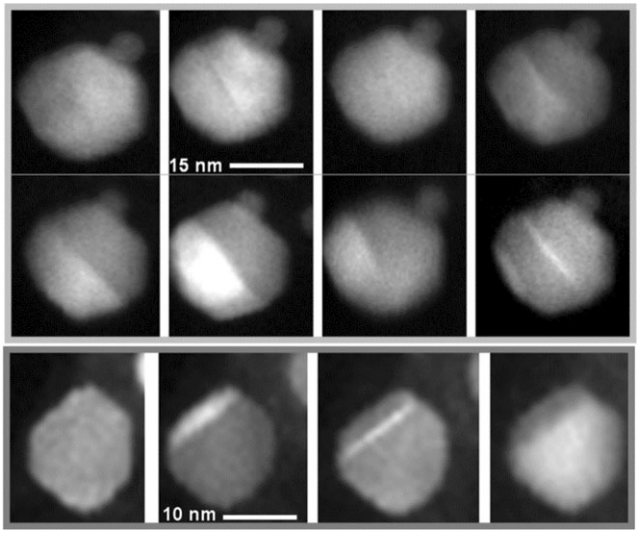

Fig. 3. Top two rows: HAADF images of a Pt particle showing different contrast at different specimen tilt angles, acquired using an inner detector semi-angle of ~50 mrad at 200 kV. Bottom row: ADF images of a Pt_3Co particle acquired using an inner detector semi-angle of ~10 mrad at 200 kV.

of images was high (~50 mrad), the contrast displays abrupt changes for different orientations of the particle.

The majority of previous HRTEM structural observations and MD simulations have involved the study of small particles that can have metastable structures, from which misleading conclusions about the equilibrium forms of larger crystals may be drawn. The MTP-to-single-twin transition has been reported to occur in Au in the 2–3 nm range [27]. Although no such studies have been performed for Pt or Pt_3Co, significantly larger MTPs are seen frequently in the present samples.

Three-dimensional shapes of LTPs

HAADF STEM tomography was used to determine the three-dimensional shapes of symmetrically and asymmetrically twinned crystals similar to those shown in Figs. 1 and 2. Figures 4 and 5 summarize results obtained from symmetrically twinned Pt and Pt_3Co particles using different approaches. The angles between the facets on the particles measured from the three-dimensional reconstructions are consistent with the modified Wulff model for twinned particles described by Marks [28]. The results also confirm that the observed twins form on 111-type planes, and that the particles have primarily 111-type surfaces. Although the resolution of the STEM tomographic reconstructions was not sufficient to resolve possible re-entrant surfaces at twins, HRTEM and STEM images such as those shown in Fig. 4c and e confirm their presence.

Figure 6 illustrates the analysis of a twinned 20 nm Pt particle. The three-dimensional shape of the particle obtained using HAADF STEM tomography is a modified cuboctahedron, in which the twins are parallel to a 111 facet

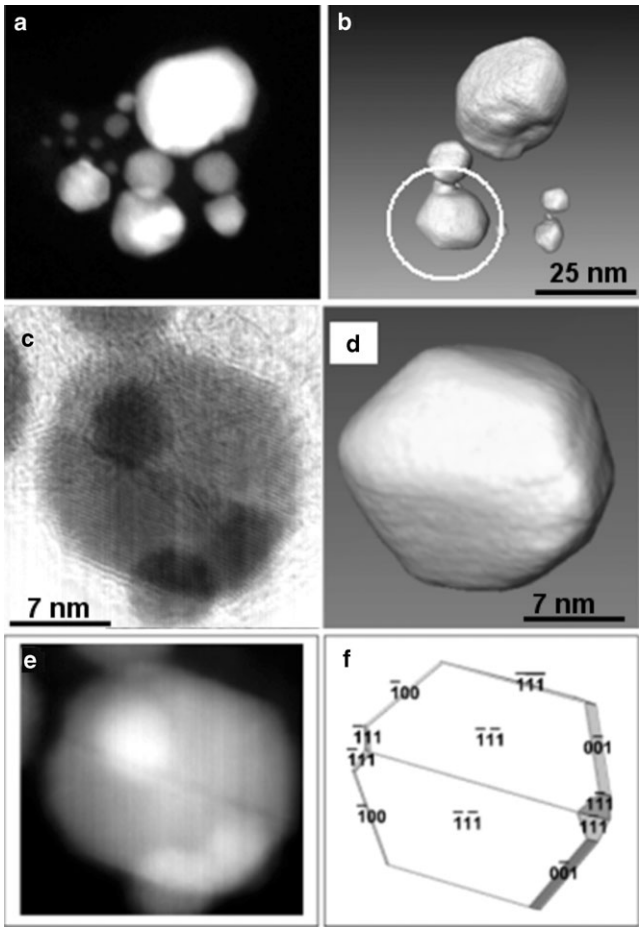

Fig. 4. (a) HAADF image taken from a tilt series of images of Pt particles supported on carbon. (b) Isosurface visualization of a three-dimensional reconstruction obtained from a tilt series of images such as that shown in (a) optimized to fit the shape of the particle inside the white circle. (c) C_s-corrected bright-field STEM image of a symmetrically twinned Pt_3Co particle obtained using a C_s-corrected VG HB501 dedicated STEM operated at 100 kV. (d) Three-dimensional shape of the particle shown in (c) obtained from an HAADF tomographic series of 70 images (−72° to +65°; 1° step) acquired using an inner detector semi-angle of ~40 mrad at 200 kV. (e) HAADF image of the Pt_3Co particle shown in (c). (f) Inferred possible crystallographic details of the twinned particle shown in (c) and (e).

(Fig. 6c and e). The measured angles between the facets and the edges of the particle, both in the tomographic reconstruction and in the original tilt series of HAADF images, were used to assign the indices of the faces on the particle that are marked in Fig. 6f.

For twinned particles, it is necessary to distinguish between thermodynamic growth (resulting in decahedral and icosahedral particles) and kinetic growth (resulting in singly and lamellar-twinned particles). The coalescence of particles can also lead to the formation of twin boundaries, as shown in Fig. 7d. While MTPs are metastable structures for smaller particles, it has been reported that lamellar twinning is preferred strongly in larger particles, even though the energy cost is expected to be zero or slightly positive, as a result

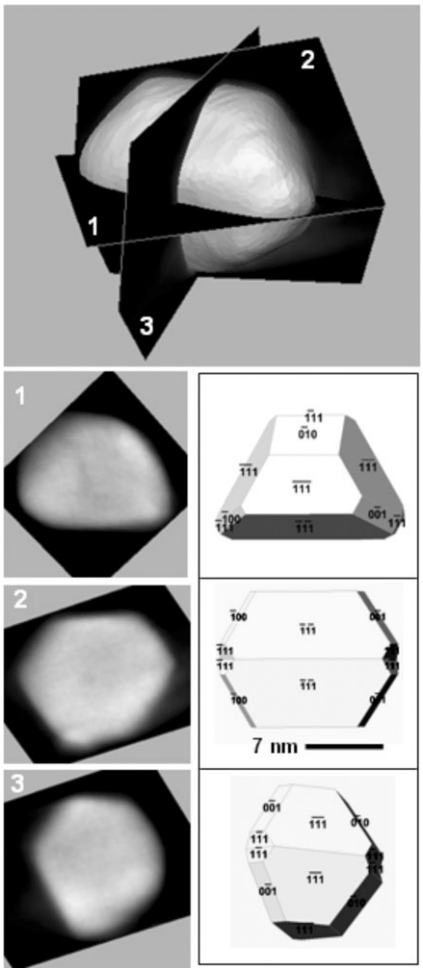

Fig. 5. Orthogonal sectioning of the tomographic reconstruction of the twinned Pt_3Co particle shown in Fig. 4d and corresponding inferred possible crystallographic models.

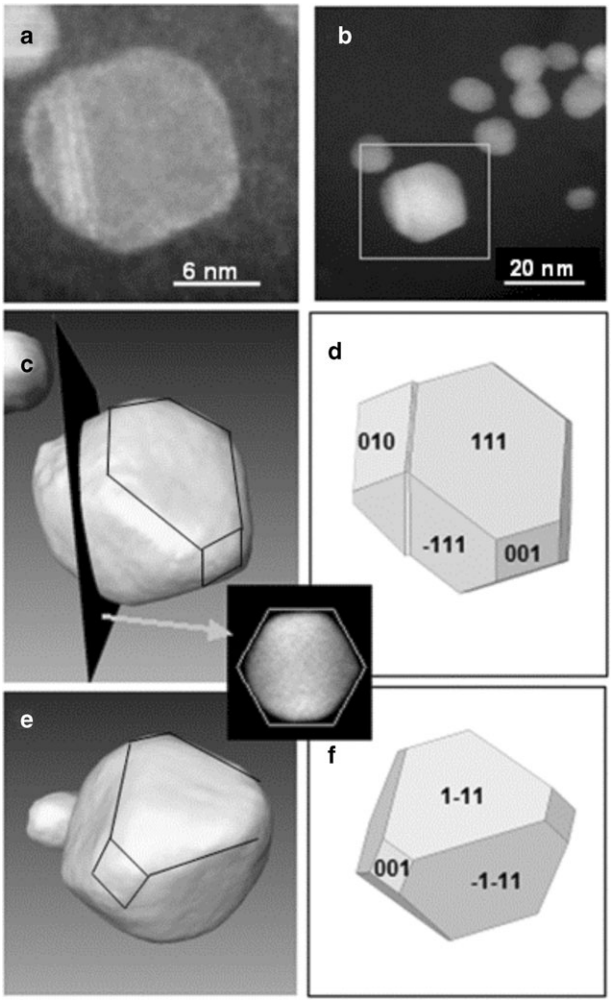

Fig. 6. (a) ADF STEM image of the Pt particle shown in (b) acquired at high magnification using an inner detector semi-angle of ~10 mrad. Bright lines across the particle arise from lamellar twinning. (b) HAADF STEM image of Pt particles acquired at 200 kV taken from a series of images acquired using a tilt range of ± 70° with a tilt increment of 2°, at a magnification of 1.3 Mx, using an inner detector semi-angle of ~40 mrad. (c and e) Two different views of the three-dimensional reconstruction of the particle shown in (a) determined using HAADF STEM tomography. (d and e) Corresponding views of the inferred modified Wulff construction. The inset between images (c)–(f) shows that a section taken through the reconstruction at the position of the twin is approximately hexagonal in shape.

of the presence of residual stresses accumulated during growth (i.e. they may be 'annealing twins') [29]. Vogel *et al.* showed that MTPs with 5-fold symmetries (decahedra and icosahedra) disappear progressively with increasing particle size and are replaced by singly twinned fcc particles [30]. Such structural changes result from a competition between surface and bulk energies, with the effects of temperature making twins move or disappear [31]. Interestingly, asymmetrically twinned particles (e.g. particle 4 in Fig. 2) are also observed, suggesting that kinetic effects are involved in their growth.

In general, the effect of temperature and adsorbates on the shapes of supported metal particles can stabilize one or more crystal planes. Supported metal particles that have been subjected to severe heat treatments (e.g. particles that have been exposed to ageing in real vehicle exhausts) can grow abnormally as a result of kinetic factors. For example, in Pt samples that have been heated in oxygen at 800°C, large platelet-like particles that contain twin planes can form. In this case, the primary growth site is the twin re-entrant edge, which provides a preferential nucleation site for incoming atoms. The particles that are studied here were subjected to heat treatments, and can therefore be classified as fast-growing particles according to the terminology of Harris [5]. Their growth constitutes a major cause of catalyst surface area loss. Such particles are more common in samples that were heated in the presence of oxygen, with the twin plane re-entrant edges then being the most likely growth sites. The presence of parallel twins in a cubic crystal may result in the formation of surface grooves that provide preferential nucleation sites for incoming atoms. Accelerated growth may

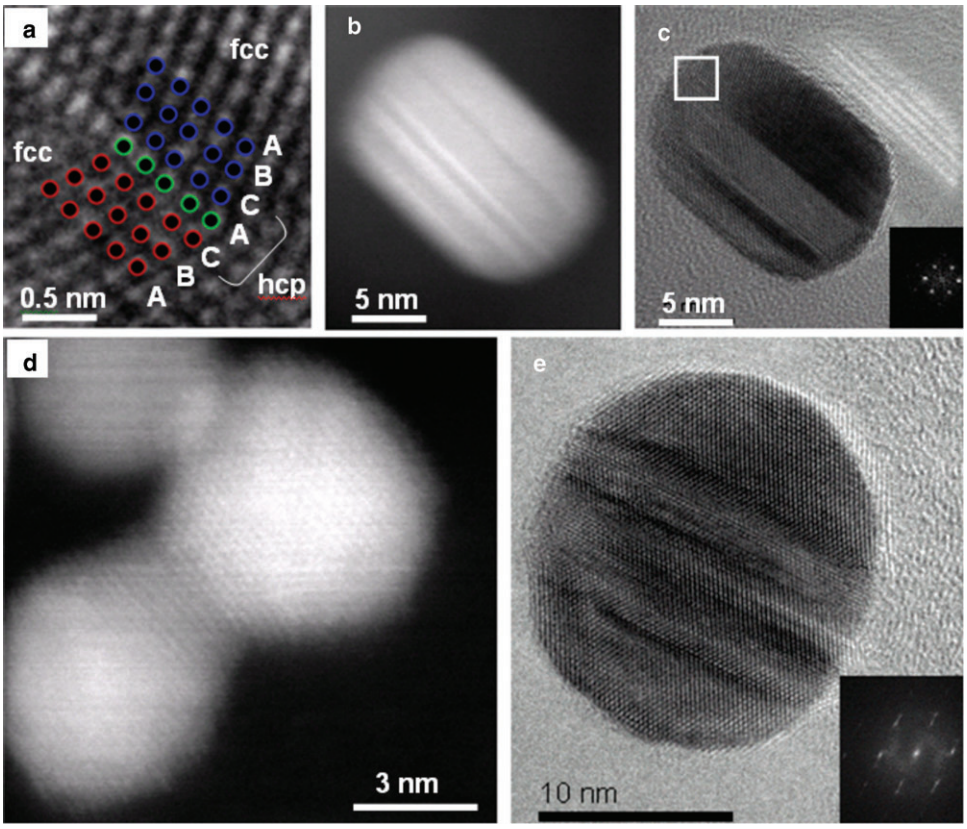

Fig. 7. (a) Atomic structure at a 111-type twin boundary marked in the Au particle shown in (c). (b and c) ADF STEM (~40 mrad inner detector semi-angle) and HRTEM images of the same lamellar-twinned Au particle. In (c), strong delocalized diffraction contrast confirms the presence of multiple grains that each have a thickness of a few atomic layers. (d) Atomic-resolution HAADF STEM (~70 mrad inner detector semi-angle) image showing two Pt particles in slightly different orientations that have coalesced. (e) HRTEM image of a rounded Au particle exhibiting lamellar twinning. The diffractogram contains streaks as a result of the presence of the lamellar twins.

then occur in a direction parallel to the twins, resulting in the formation of large platelet-like particles.

Figures 7a–c show examples of images of rapidly grown platelet-like particles of Au, which contain parallel twins that each have a thickness of a few atomic layers, as previously reported for Ag [22]. It has been suggested that alloying may reduce some of the problems that result from abnormally rapid growth if the alloy increases the twin boundary energy at the grooves. However, our results show that twinned particles, and in particular LTPs, are found more frequently in Pt_3Co than in pure Pt, suggesting either that Pt_3Co has a lower twin boundary energy than Pt or that the particles form from MTPs.

Contrast features in ADF images of twinned particles

The origin of the contrast observed in lamellar-twinned Pt and Pt alloy nanoparticles such as that shown in Fig. 3 is now discussed. Examples of similar contrast features are also visible in HRTEM and HAADF images of Au particles. Many of the particles show abrupt changes in contrast at boundaries between adjacent grains, which may result from diffraction effects related to particle orientation or from strain resulting from imperfection of the crystal structures at the boundaries. The suggestion that MTPs are made up of inhomogeneously strained single crystal units [32] has recently been confirmed experimentally for Au nanoparticles by using geometrical phase analysis [21]. The HRTEM image of a Au LTP shown in Fig. 7e contains complicated contrast that originates from a combination of Moiré fringes (see also Fig. 2c) and defects. The presence of Moiré fringes does not alone provide evidence that inhomogeneous strains are not also present in LTPs [20]. High-order grain boundaries and twins do not in general correspond to absolute minima in energy, and may be associated with distortions of atomic planes close to the boundaries [33]. Indeed, the stability and migration of grain boundaries (twins) in Au particles [34] and lattice distortions and shear moduli at coherent twin boundaries [35] have both been discussed. While high-order grain boundaries may be ejected after irradiation with a high-energy electron beam, coherent twin boundaries similar to those reported in this paper appear to be more stable.

ADF contrast usually depends on a combination of specimen thickness, composition, orientation and detector inner angle. The presence of thermal diffuse scattering (TDS)

and multiple scattering makes the quantitative interpretation of the contrast difficult. Resonant phonon modes can occur close to twin boundaries and enhance TDS [33], and localized static strain can give rise to ADF contrast similar to that arising from variations in composition or thickness. Indeed, Perovic *et al*. [36] showed that ADF images of B-doped silicon can exhibit opposite contrast to that expected as a result of scattering from displaced atoms surrounding impurity atoms. Figure 6a shows an ADF STEM image of a Pt particle acquired using an inner detector collection angle of ~10 mrad in order to enhance diffraction contrast. This particle is asymmetrically twinned and crossed by three bright lines that may be parallel twins. Interestingly, the edge of the Pt particle is also bright, possibly as a result of strain resulting from a surface contraction measured experimentally for Pt nanoparticles [37]. As the particle is pure Pt, such variations in contrast are unlikely to be associated with compositional variations.

Elastic contrast can be preserved in HAADF images as a result of channelling along planar or axial directions in crystals. Unless the annular HAADF detector has a large inner acceptance angle (>40 mrad), it will collect a significant proportion of coherent (Bragg) scattering. For example, grain boundary dislocations may exhibit complicated contrast, going from dark at the entrance surface of the specimen to oscillatory and finally to bright at the exit surface [38]. Similarly, contrast at twin planes in LTPs of fcc crystals can be understood with reference to the Ewald sphere. 111-type twins in fcc crystals are stacking faults, as shown in Fig. 7a, and separate grains contain a common reflection. A perfect boundary will define a thin platelet with an hcp structure, i.e. a planar fault. In the reciprocal lattice, this fault will result in an elongated relrod perpendicular to the hcp platelet, which is excited when the particle is tilted.

Concluding remarks

High-tilt series of low-angle ADF STEM images can be used to image crystal domains in twinned nanoparticles rapidly with a high signal-to-noise ratio and a large field of view, providing statistically meaningful data that can be correlated with other techniques such as HRTEM. Here, such images are used to show that Pt and Pt alloy particles are twinned frequently. The presence of such twins may result in XRD measurements of particle sizes that are, in general, smaller than those measured using TEM [39]. The acquisition of tilt series of ADF images using low collection angles to enhance diffraction contrast can be very useful for understanding the structures of non-single-crystalline samples with complicated structures.

Both symmetrically and asymmetrically twinned particles are observed, with a greater frequency of twins in alloy particles. The sizes of the twinned Pt particles studied here are frequently larger than those observed in previous studies for Au, possibly as a result of the coalescence of particles during growth. The three-dimensional shapes of symmetrically and asymmetrically twinned particles, which contain 111 twin planes, have been measured using HAADF STEM tomography. Although the spatial resolution of HAADF STEM tomography does not allow re-entrant grooves to be imaged in three dimensions, their presence can be confirmed using HRTEM. Contrast features in HAADF and ADF STEM images of LTPs may originate in part from strain and diffraction contrast that is preserved even when a large detector collection semi-angle is used. Future studies would benefit from the combined use of HAADF STEM tomography with geometrical phase analysis and detailed simulations of contrast in HAADF and ADF STEM images.

Funding

We are grateful to the EPSRC (UK) for financial support and also to the European Union under a contract for an Integrated Infrastructure Initiative (reference 026019 ESTEEM).

Acknowledgements

The authors wish to thank David Thompsett, Steve Spratt, Gregory Goodlet, Tim Hyde and Peter Ash from Johnson Matthey, and Paul A. Midgley of the Department of Materials Science and Metallurgy in Cambridge (UK) for useful discussions, and Angus I. Kirkland and Crispin J. D. Hetherington of the Department of Materials in Oxford (UK) for valuable assistance and discussions.

References

1 Murray W, and Barnes W L (2007) Plasmonic materials. *Adv. Mater.* **19**: 3771–3782.

2 Ou H, Rørdam T P, Rottwitt K, Grumsen F, and Horsewell A (2006) Ge-nanoclusters embedded in Ge-doped silica-on-silicon waveguides. *Electron. Lett.* **42**: 532–534.

3 Hartland G V (2007) Is perfect better? *Nat. Mater.* **6**: 716–717.

4 Marks L D (1994) Experimental studies of small particle structures. *Rep. Prog. Phys.* **57**: 603649.

5 Harris P J F (1995) Growth and structure of supported metal catalyst particles. *Int. Mater. Rev.* **40**: 97–115.

6 Ajayan P M, and Marks L D (1988) Quasimelting and phases of small particles. *Phys. Rev. Lett.* **60**: 585–587.

7 Gordon M B, Cyrot-Lackmann F, and Desjonqueres M C (1979) Relaxation and stability of small transition metal particles. *Surf. Sci.* **80**: 159–164.

8 Khanna S N, Bucher J P, Buttet J, and Cyrot-Lackmann F (1983) Stability and lattice contraction of small platinum particles. *Surf. Sci.* **127**: 165–174.

9 Hall B D, Flüeli M, Monot R, and Borel J (1991) Multiply twinned structures in unsupported ultrafine silver particles observed by electron diffraction. *Phys. Rev. B* **43**: 3906–3917.

10 Wang Y, Teitel S, and Dellago C (2004) Melting and equilibrium shape of icosahedral gold nanoparticles. *Chem. Phys. Lett.* **394**: 257–261.

11 Cleveland C L, Luedtke W D, and Landman U (1999) Melting of gold clusters. *Phys. Rev. B* **60**: 5065–5077.

12 Reinhard D, Hall B D, Berthoud P, Valkealahti S, and Monot R (1998) Unsupported nanometer-sized copper clusters studied by electron diffraction and molecular dynamics. *Phys. Rev. B* **58**: 4917–4925.

13 Reinhard D, Hall B D, Berthoud P, Valkealahti S, and Monot R (1997) Size-dependent icosahedral-to-fcc structure change confirmed in unsupported nanometer-sized copper clusters. *Phys. Rev. Lett.* **79**: 1459–1462.

14 Ino S, Ogawa S, Taoka T, and Akahori H (1972) A study of multiply-twinned particles by 1000 kV electron microscope. *Japan. J. Appl. Phys.* **11**: 1859–1859.

15 Monosmith W B, and Cowley J M (1984) Electron microdiffraction from very small gold particles. *Ultramicroscopy* **12**: 177–183.

16 Solliard C (1981) Structure and strain of the crystalline lattice of small gold and platinum particles. *Surf. Sci.* **106**: 58–63.

17 Reinhard D, Hall B D, Berthoud P, Valkealahti S, and Monot R (1998) Unsupported nanometer-sized copper clusters studied by electron diffraction and molecular dynamics. *Phys. Rev. B* **58**: 4917–4925.

18 Kaszkur Z (2000) Powder diffraction beyond the Bragg law, study of palladium nanocrystals. *J. Appl. Cryst.* **33**: 1262–1270.

19 Yacamán J M, and Ocaña T (1977) High-resolution dark-field electron microscopy of small metal particles. *Phys. Stat. Solidi A* **42**: 571–577.

20 Marks L, and Smith D J (1981) High resolution studies of small particles of gold and silver: II. Single crystals, lamellar twins and polyparticles. *J. Cryst. Growth* **54**: 433–438.

21 Johnson C L, Snoeck E, Ezcurdia M, Rodríguez-González B, Pastoriza-Santos I, Liz-Marzán L M, and Hÿtch M J (2008) Effects of elastic anisotropy on strain distributions in decahedral gold nanoparticles. *Nat. Mater.* **7**: 120–124.

22 Hofmeister H, Dubiel M, Tan G L, and Schicke K-D (2005) Configuration of twins in glass-embedded silver nanoparticles of various origin. *Phys. Stat. Solidi A***202**: 2321–2329.

23 Coloma F, Sepúlveda-Escribano A, and Rodríguez-Reinoso (1995) Heat-treated carbon blacks as supports for platinum catalysts. *J. Catal.* **154**: 299–305.

24 Xiong L, and Manthiram A (2004) Influence of atomic ordering on the electrocatalytic activity of Pt-Co alloys in alkaline electrolyte and proton exchange membrane fuel cells. *J. Mater. Chem.* **14**: 1454–1460.

25 Midgley P A, Weyland M, Yates T J V, Arslan I, Dunin-Borkowski R E, and Thomas J M (2006) Nanoscale scanning transmission electron tomography. *J. Microsc.* **223**: 185–190.

26 Cervera-Gontard L, Dunin-Borkowski R E, and Ozkaya D (2008) Three-dimensional shapes and spatial distributions of Pt and PtCr catalyst nanoparticles on carbon black. *J. Microsc.* **232**: 248–259.

27 Cleveland C L, Landman U, Shafigullin M N, Stephens P W, and Whetten R L (1997) Structural evolution of larger gold clusters. *Zeitschrift für Physik D* **40**: 503–508.

28 Marks L D (1983) Modified Wulff construction for twinned particles. *J. Cryst. Growth* **61**: 556–566.

29 Cleveland C L, Landman U, Schaaff T G, Shafigullin M N, Stephens P, and Whetten, R L (1997) Structural evolution of smaller gold nanocrystals: the truncated decahedral motif. *Phys. Rev. Lett.* **79**: 1873–1876.

30 Vogel W, Bradley J, Vollmer O, and Abraham I (1998) Transition from five-fold symmetric to twinned fcc gold particles by thermally induced growth. *J. Phys. Chem. B* **102**: 10853–10859.

31 Marks L D (1983) Modified Wulff construction for twinned particles. *J. Cryst. Growth* **61**: 556–566.

32 Howie A, and Marks L D (1984) Elastic strains and the energy balance for multiply twinned particles. *Philos. Mag. A* **49**: 95–109.

33 Hasimoto M, Ichinose H, Ishida Y, Yamamoto R, and Doyama M (1980) The simulated and observed structure of a $\Sigma = 11$ tilt boundary in gold and the vibrations of individual atoms at the grain boundary. *Japan. J. Appl. Phys.* **19**: 1045–1050.

34 Ijima S, and Ichihashi T (1987) Grain boundary migration in small gold particles. *Surf. Sci.***192**: 872–878.

35 Suesawa M, and Sumino K (1976) Lattice distortion and the effective shear modulus along a coherent twin boundary. *Phys. Stat. Solidi A* **36**: 263–268.

36 Perovic D D, Rossouw C J, and Howie A (1993) Imaging elastic strains in high-angle annular dark field scanning transmission electron microscope. *Ultramicroscopy* **52**: 353–359.

37 Wasserman H J, and Vermaak J S (1972) On the determination of surface stress of copper and platinum. *Surf. Sci.* **32**: 168–174.

38 Hillyard S, and Silcox J (1995) Detector geometry, thermal diffuse scattering and strain effects in ADF STEM imaging. *Ultramicroscopy* **58**: 6–17

39 Cervera Gontard L, Dunin-Borkowski R E, Ozkaya D, Hyde T, Midgley P A, and Ash P (2005) Crystal size and shape analysis of Pt nanoparticles in two and three dimensions. *J. Phys: Conf. Ser.* **26**: 367–370.